Report on HOSTS survey return

S. Ertel[1], P. Hinz[1], B. Mennesson[2], D. Defrère[3], G. Kennedy[4,5], P. Willems[2], and the HOSTS science team

1 Scope of this Document

Observations for the HOSTS (Hunt for Observable Signatures of Terrestrial Systems) survey for warm dust around nearby stars (exozodiacal dust, i.e., dust in and near their habitable zones, HZs) have been completed in the first half of 2018 (during observing semester 2018A). The goal of HOSTS was to constrain the occurrence rate and typical level of exozodiacal dust around a sample of nearby stars in order to assess the risk imposed by this dust to future space missions attempting to directly image habitable exoplanets. We here report on the immediate conclusions of the survey relevant to this goal.

Detailed descriptions of the HOSTS observing strategy, data reduction, and analysis together with detailed statistical results were provided by Ertel et al. (2018a). Here, we provide only a brief summary of these points and updates where necessary. In particular, we provide the final null measurements and derived HZ dust levels (zodi levels) for all observed stars and final statistics derived from those measurements.

2 Observations

The observations have been carried out with the Large Binocular Telescope Interferometer (LBTI). We used nulling interferometry in the N band to combine the two 8.4m apertures, to suppress the light from the central star, and to reveal faint, circumstellar emission. The total flux transmitted in nulling mode was measured and calibrated using a photometric observation of the target star. Nodding was used to subtract the variable telescope and sky background. Each observation of a science target (SCI) was paired with an identical observation of a reference star (CAL) to determine the instrumental null depth (nulling transfer function, the instrumental response to a point source) and calibrate the science observations.

Science targets were selected from the full HOSTS target list compiled by Weinberger et al. (2015) according to target observability and priority. This list consists of nearby, bright ($N > 1$ Jy) main sequence stars without close binary companions (within 1.5″). The sample is separated into early type stars (spectral types A to F5) for which our observations are most sensitive and Sun-like stars (spectral types F6 to K8) which are preferred targets for future exo-Earth imaging missions. The observed stars are listed with their basic properties in Table 1. Calibrators were selected following Mennesson et al. (2014) using the catalogs of Bordé et al. (2002) and Mérand et al. (2005), supplemented by stars from the JSDC catalog and the SearchCal tool (both Chelli et al. 2016) where necessary. Several calibrators (usually four) were selected for each science target so that the same calibrator was typically not used twice for the same science target in order to minimize systematic errors due to imperfect knowledge of

[1]Steward Observatory, Department of Astronomy, University of Arizona, 933 N. Cherry Ave., Tucson AZ 85721, USA
[2]Jet Propulsion Laboratory, California Institute of Technology, 4800 Oak Grove Dr., Pasadena CA 91109, USA
[3]Space Sciences, Technologies & Astrophysics Research (STAR) Institute, University of Liège, Liège Belgium
[4]Department of Physics, University of Warwick, Gibbet Hill Road, Coventry CV4 7AL, UK
[5]Institute of Astronomy, University of Cambridge, Madingley Road, Cambridge CB3 0HA, UK

the calibrator stars.

Observations were carried out in queue mode together with a variety of other observing programs using the LBTI, including high-contrast direct imaging and integral field spectroscopic observations. This increased the pool of nights to choose from for the nulling observations which are very demanding in terms of weather conditions. A total of ten nights of observing time per observing semester were allocated for the HOSTS survey over the 2016B, to 2018A semesters. To ensure progress on the HOSTS survey could be made as expected, four nights per semester were allocated as highest priority in the queue, to be executed when ever the weather was suitable. The remaining six nights per semester were allocated as lower priority and served in part as contingency for weather loss.

3 Data reduction and zodi measurements

Data reduction followed the strategy outlined by Defrère et al. (2016) with minor updates as described by Ertel et al. (2018a). After a basic reduction of each frame (nod subtraction, bad pixel correction), aperture photometry was performed on each single frame. Three different apertures were used to (1) optimize the photon and read noise limited signal-to-noise in the aperture assuming emission that is spatially unresolved by the single dish telescope PSF, (2) optimize the photon and read noise limited signal-to-noise for extended emission analogous to the Solar system zodiacal dust, and (3) include all plausible extended N band dust emission from the system. The raw null depths and their uncertainties were determined using the null self calibration method (NSC, Mennesson et al. 2011; Hanot et al. 2011; Defrère et al. 2016; Mennesson et al. 2016), combining all frames recorded within a given nod for a statistical analysis. These measurements within an observing sequence of a science target were then combined and the corresponding calibrator observations were used to calibrate the null measurements. The calibrated null measurements for each aperture and each science target are listed in Table 1.

For the conversion from null measurements to dust levels, we used the model presented by Kennedy et al. (2015). It describes a radial dust surface density distribution analogous to the Solar system's zodiacal dust, scaled in size with the square root of the host star's luminosity. We scale the dust surface density (vertical geometrical optical depth) of this model to 7.17×10^{-8} at the Earth Equivalent Insolation distance (EEID, the distance from the star where a body receives the same energy density from the star as Earth does from the Sun), equal to the surface density of the zodiacal dust at 1 AU from the Sun. This defines the unit of 1 zodi which we use to quantify the HZ dust levels around our target stars.

The usually unknown orientation of the potential dust disk (inclination and position angle) were randomized and the response of the LBTI to all possible orientations was used to compute a most likely null-to-zodi conversion factor and its uncertainty from the typically unknown disk orientation. Correction factors for the limited aperture size were computed from the same model. For detected excesses we converted the null measurement from the aperture that yields the most significant detection to a zodi level. For non detections we used the measurement based on the noise optimized aperture assuming a dust distribution analogous to the Solar system's zodiacal dust. This assumption is justified by the fact that our detections all agree with it within the measurement uncertainties.

4 Results

The null and zodi measurements derived from the HOSTS survey are listed in Table 1. Fig. 1 shows the null measurements and sensitivities reached for all stars and the three apertures used. The distributions

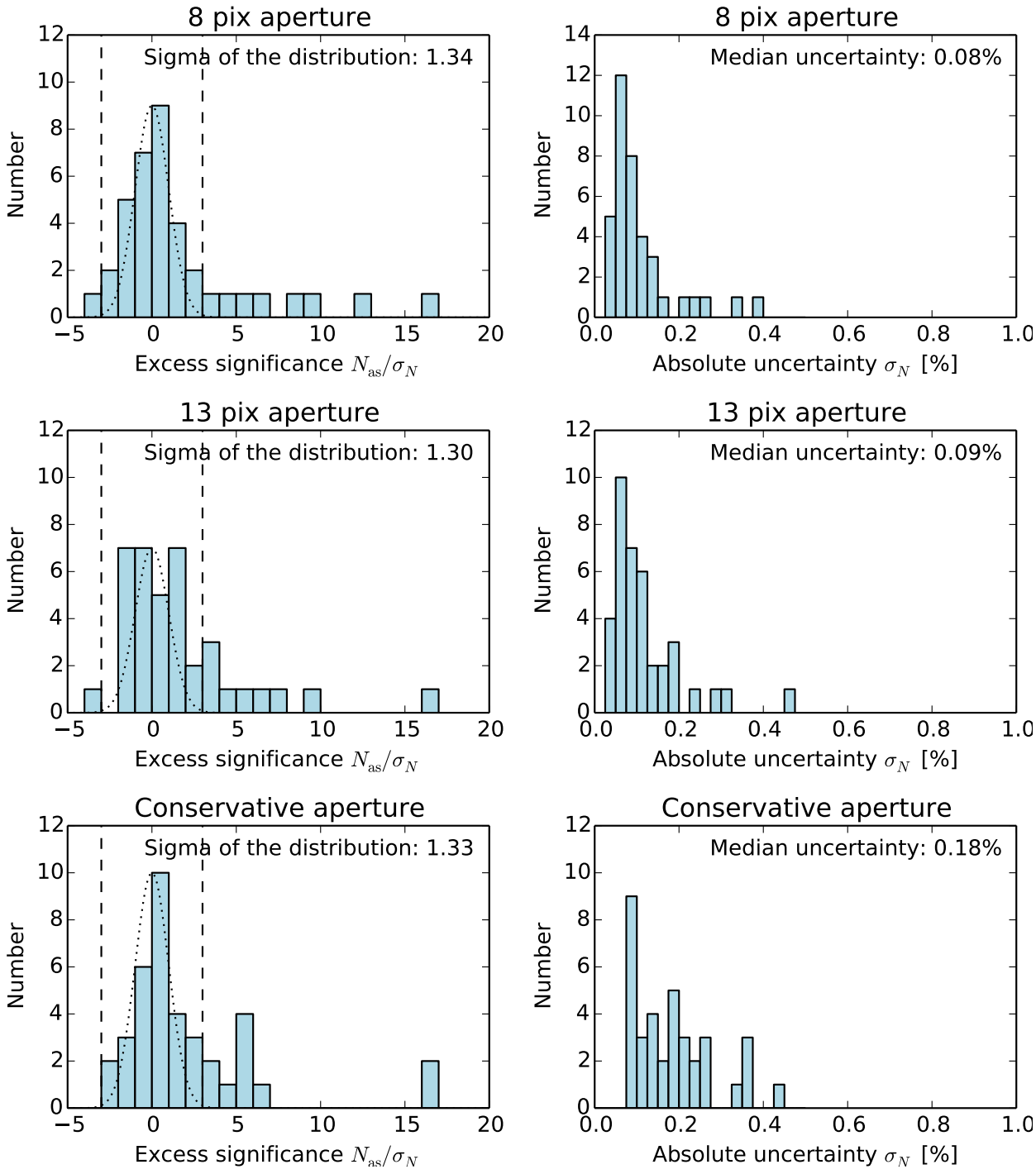

Fig. 1: Histograms of null measurements and uncertainties for all hosts survey observations.

Table 2: Subsamples, excess detections, and occurrence rates.

	Cold dust	Clean	All
Early type	5 of 6 $83^{+6}_{-23}\%$	1 of 9 $11^{+18}_{-4}\%$	6 of 15 $40^{+13}_{-11}\%$
Sun-like	1 of 2 $50^{+25}_{-25}\%$	3 of 20 $15^{+11}_{-5}\%$	4 of 23 $17^{+10}_{-5}\%$
All	6 of 8 $75^{+9}_{-19}\%$	4 of 29 $13^{+9}_{-4}\%$	10 of 38 $26^{+8}_{-6}\%$

of the significance $N_{\rm as}/\sigma_N$ of null measurements are generally well behaved, consistent with a Gaussian distribution around a significance of $N_{\rm as}/\sigma_N = 0$ and a tail of detections at $N_{\rm as}/\sigma_N > 3$. This can be expected for a sample in which a fraction of stars have no excesses, while the other stars do have significant excess. The standard deviation of the Gaussian distribution (measured for stars with $N_{\rm as}/\sigma_N < 3$) is slightly larger than the expected value of one by a factor of ∼1.3. This may indicate that among the stars without significant null excess there are still stars with tentative excesses, or that we slightly underestimate our measurement uncertainties. While the former can be expected, the latter is also supported by the one measurement of $N_{\rm as}/\sigma_N < -3$ and the generally symmetrical distribution of non-detections around $N_{\rm as}/\sigma_N = 0$. The distribution of the measurement uncertainties is also well behaved with a sharp peak at low uncertainty and a tail toward higher uncertainties for stars observed under less suitable conditions or for which the observations could not be completed. As expected, the median uncertainty increases with aperture size. The larger scatter for the conservative aperture can be explained by the fact that this aperture is optimized for each star and thus changes from target to target.

Based on these arguments, we define our detection threshold as $N_{\rm as}/\sigma_N > 3$. We detect such excesses around 10 stars among the total of 38 stars observed. These stars show strong excess ($N_{\rm as}/\sigma_N > 5$) and/or have been detected combining consistent data from at least two independent observations (i.e., in at least two different nights). Another star, 13 UMa, shows a tentative detection. However, due to mediocre data quality and partly inconsistent results from two independent observations and for different aperture sizes, we do not consider this detection significant.

It is interesting to note that the data quality has been improving continuously throughout the survey due to better understanding of the instrument performance, telescope vibrations, and weather constraints, as well as improved experience in executing the observations. This is most evident when comparing the median null uncertainty for a given aperture size in Fig. 1 for the whole sample with that of the early sample published by Ertel et al. (2018a). For example, for our nominal (13 pix) aperture the median uncertainty has been improved from 0.11% to 0.09%. In addition, several ongoing and future upgrades (e.g., adaptive optics, new detector) are expected to further improve performance.

The basic detection statistics for different subsamples of targets are summarized in Table 2. We find higher detection rates for stars with cold dust (dusty stars) compared to stars without (clean stars). For early type stars this correlation is strong, but the small number of dusty Sun-like stars in our sample prohibits a definite conclusion. Such stars are relatively rare and observing them was not a priority of the HOSTS survey as stars with known cold dust are unlikely to be first choice targets for future exo-Earth imaging missions.

Fig. 2 compares the zodi sensitivities (1σ accuracy of the measurements) reached by the HOSTS

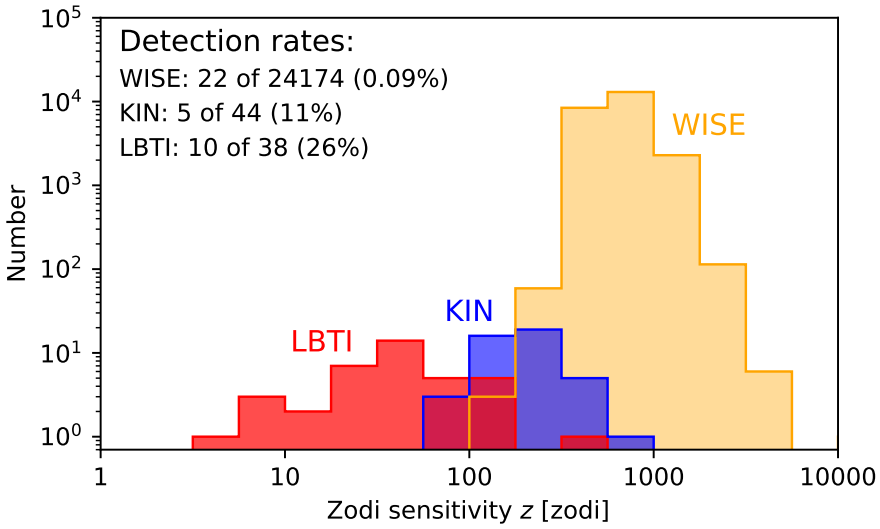

Fig. 2: Sensitivity of the HOSTS survey compared to previous surveys.

survey to those of previous surveys, specifically the photometric measurements from WISE (Kennedy & Wyatt, 2013) and the Keck Interferometer Nuller (KIN; Mennesson et al. 2014). We can see that our sensitivity is about a factor 5 better than that of KIN for the observed samples. It is also visible that for our best targets we are now able to detect HZ dust levels that are only a few times higher than in our Solar system. Thus, using our Solar system as a template, the LBTI is now the most sensitive facility to detect dust disks around a sample of most favorable stars.

5 Sample constraints on habitable zone dust levels

In addition to the basic statistics described in the previous section, we carried out a detailed statistical analysis to determine the typical HZ dust level for Sun-like stars. We followed the strategy described by Mennesson et al. (2014) and Ertel et al. (2018a). In our previous analysis of an early subset of HOSTS observations, we assumed a log-normal probability distribution of the zodi level of a given star (luminosity function) and fitted it to our zodi measurements for different subsamples of stars to determine the median zodi levels of these samples and its uncertainties. We found that: (1) a lognormal luminosity function appears inadequate to reproduce the observed distribution of excesses well, instead a bimodal luminosity function in which most stars have low zodi levels and a few 'outliers' have relatively high levels is more likely, and (2) within our statistical uncertainties, the difference between stars with and without cold dust seen for early-type stars cannot be confirmed or ruled out for Sun-like stars. The former is further supported by our complete survey data, while the latter remains valid. We thus do not distinguish between dusty and clean Sun-like stars and use the 'free-form' iterative maximum likelihood algorithm described by Mennesson et al. (2014) instead of a lognormal luminosity function.

For the free-form method, the explored zodi levels are binned and the unknown luminosity function is parameterized through the probability that a given star has a zodi level in each of the bins. For our analysis we selected bins of equal width of 1 zodi ranging from 0 zodis to 2000 zodis, an upper limit consistent with the LBTI measurements of Sun-like stars. The probability in each bin was then adjusted iteratively to maximize the likelihood of observing the data (Mennesson et al. 2014, Section 4.6). The

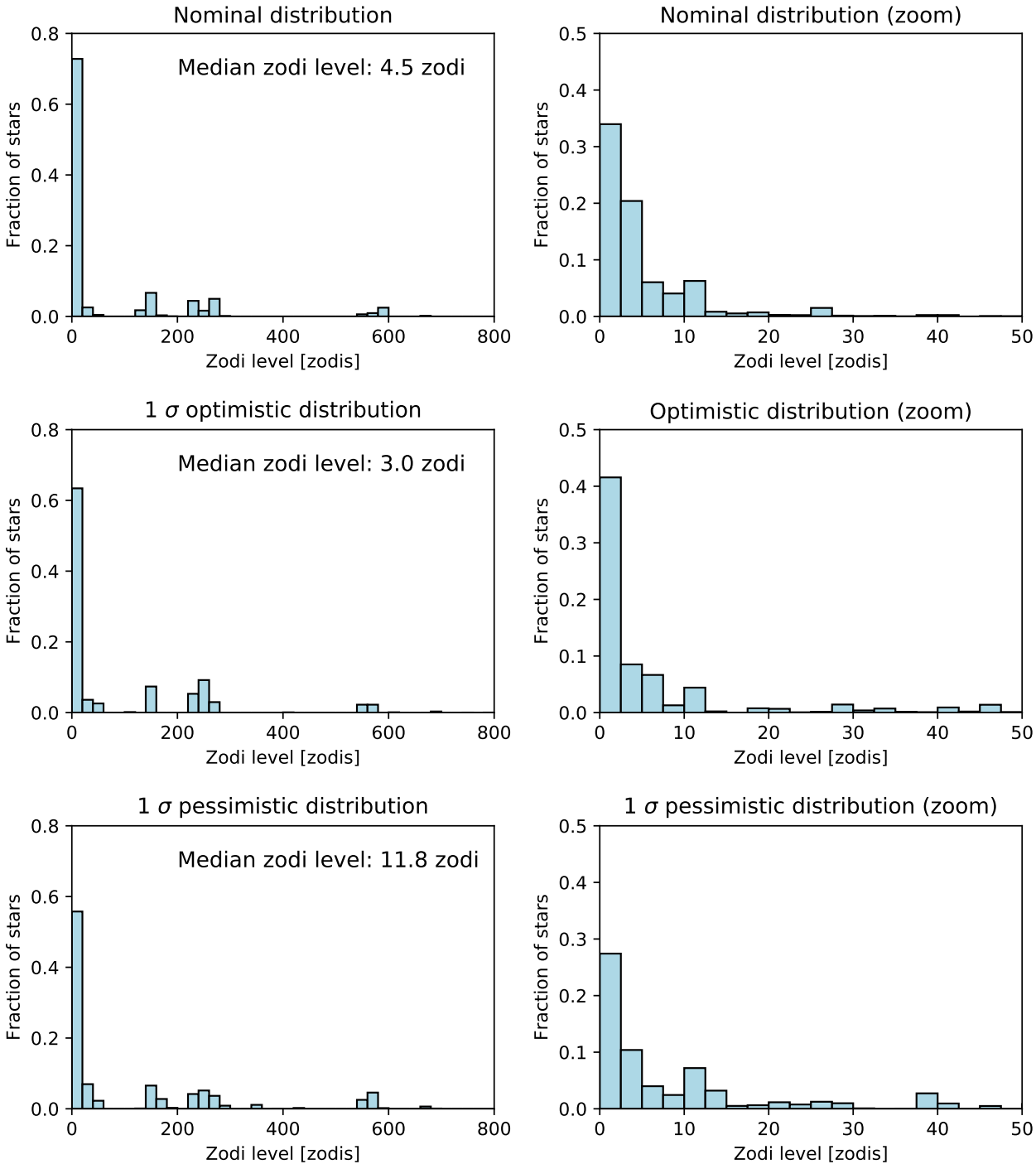

Fig. 3: Nominal, optimistic (low median, $m - \sigma_{\text{lower}}$), and pessimistic (high median, $m + \sigma_{\text{upper}}$) free form fits to the HOSTS data for Sun-like stars.

median zodi level m was used to characterize the distribution. To determine the uncertainty of the derived distribution, we randomly disturbed this 'nominal' distribution, creating 10^5 new distributions with small deviations form the nominal one. The likelihood of observing the data was computed for each of these distributions, and the profile likelihood theorem was then used to derive 1σ confidence intervals on m from its distribution among them. We find from our data a median zodi level of Sun-like stars of $m = 4.5^{+7.3}_{-1.5}$ zodis. The nominal and 1σ optimistic (low median, $m - \sigma_{\text{lower}}$) and pessimistic (high median, $m + \sigma_{\text{upper}}$) free-form distributions are shown in Fig. 3. These statistics have been adopted by the HabEx and LUVOIR mission study teams.

6 Detailed analysis of specific detections

In addition to the statistical constraints derived from the HOSTS observations, the data also provide important constraints on specific systems for which exozodiacal dust has been detected or for which strong and interesting upper limits have been found. β UMa and β Leo are examples of massive HZ dust detections in systems with known cold dust. In contrast, Vega has surprisingly low HZ dust level despite a massive cold disk. ϵ Eri is a nearby, interesting late type star for exo-Earth imaging, but has a very high HZ dust level, so should be avoided. The dust in the 110 Her system seems to be concentrated relatively far from the star, while the large amounts of dust around η Crv is located very close in (Defrère et al., 2015). Several systems have high HZ dust levels despite the lack of detected cold dust, which may complicate the target selection for exo-Earth imaging and needs to be understood.

These systems can be studied in detail to understand their properties and diversity of their architectures in order to understand the connection between the HZ dust level and other properties of a system such as stellar luminosity, the presence of an outer, cold dust belt, or the presence of known planets in the system. Such studies improve our understanding of the formation and evolution of the HZ dust and thus increase the ability of models to predict the level of HZ dust in systems that could not be observed by the HOSTS survey. This will critically assist in the target selection for future exo-Earth imaging missions, for example by determining whether Sun-like stars with known cold dust really need to be avoided (some of those systems such as τ Ceti would be the most interesting targets). We have performed the first such studies on the exizting data (Defrère et al. 2015, Hinz et al. in prep.) and the HOSTS science team is currently analyzing the most relevant, remaining detections. Follow-up observations with the LBTI at a wide range of position angles and different wavelengths are critical, however, to derive strong constraints on the architectures of the detected dust disks. Furthermore, the wider community has already taken up the first HOSTS publications for more analyses. Bonsor et al. (2018) have developed a model to predict or rule out the presence of giant planets in a system based on the mass and location of an outer belt and the level of HZ dust from our observations. More analyses of our detections will help calibrating this model to produce accurate constraints.

7 Conclusions

The HOSTS survey has been completed successfully. In this report we have delivered the final null and zodi measurements for all stars observed and the derived statistical constraints on the typical dust levels of nearby main sequence stars. We found a best-fit median zodi level for Sun-like stars of $m = 4.5^{+7.3}_{-1.5}$ zodis. These constraints have been adopted by the HabEx and LUVOIR mission study teams. Our results are in the regime of $\lesssim$10 zodis where they critically inform future exo-Earth imaging missions. We found a significant number of detections and detailed studies of these systems will improve our predictive power

of zodi levels for systems that could not be observed.

We showed that the performance of the LBTI has been continuously improving due to better understanding of the system and weather constraints for nulling observations. Maintaining this expertise is critical for future use of the LBTI or other nulling interferometric facilities to further inform exo-Earth imaging missions. The performance is expected to further improve in the future due to ongoing and planned instrument upgrades.

Despite the successful completion of the HOSTS survey, there are several open questions that need to be answered in the future, specifically with new, focussed LBTI observations. It needs to be determined by observing a larger sample of Sun-like stars with cold dust if these stars host significantly larger amounts of HZ dust compared to clean Sun-like stars. The diversity of exozodi systems needs to be better understood by follow-up observation and characterization of the detected systems in order to better understand the origin of the dust and strengthen the predictive power of modes of its formation and evolution. This way, the dust levels of stars that cannot be observed by the LBTI (too faint, too far South) can be better predicted. One caveat of the HOSTS observations are the weak constraints on the dust properties and thus the scattered light brightness of exozodiacal dust in the visible from the N band thermal emission observations. Characterizing the detected systems through multi-wavelength observations with the LBTI across the N band (and in principle possible down to the K band) are critical to better constrain the dust properties and to complement future scattered light observations of our brightest targets, e.g., with WFIRST. The prospects for follow-up observations of HOSTS detections with the LBTI have been discussed in detail by Ertel et al. (2018b).

This document is excerpted from an unpublished prior version that contains information of a purely contractual nature that is not included here. This research was carried out by the Jet Propulsion Laboratory, California Institute of Technology, under a contract with the National Aeronautics and Space Administration, primarily through a subcontract to the University of Arizona.

References

Bonsor, A., Wyatt, M. C., Kral, Q., et al. 2018, MNRAS, 480, 5560

Bordé, P., Coudé du Foresto, V., Chagnon, G., & Perrin, G. 2002, A&A, 393, 183

Chelli, A., Duvert, G., Bourgès, L., et al. 2016, A&A, 589, A112

Defrère, D., Hinz, P. M., Skemer, A. J., et al. 2015, ApJ, 799, 42

Defrère, D., Hinz, P. M., Mennesson, B., et al. 2016, ApJ, 824, 66

Ertel, S., Defrère, D., Hinz, P., et al. 2018a, AJ, 155, 194

Ertel, S., Kennedy, G. M., Defrère, D., et al. 2018b, in Society of Photo-Optical Instrumentation Engineers (SPIE) Conference Series, Vol. 10698, Space Telescopes and Instrumentation 2018: Optical, Infrared, and Millimeter Wave, 106981V

Hanot, C., Mennesson, B., Martin, S., et al. 2011, ApJ, 729, 110

Kennedy, G. M., & Wyatt, M. C. 2013, MNRAS, 433, 2334

Kennedy, G. M., Wyatt, M. C., Bailey, V., et al. 2015, The Astrophysical Journal Supplement Series, 216, 23

Mennesson, B., Hanot, C., Serabyn, E., et al. 2011, ApJ, 743, 178

Mennesson, B., Millan-Gabet, R., Serabyn, E., et al. 2014, ApJ, 797, 119

Mennesson, B., Defrère, D., Nowak, M., et al. 2016, in Society of Photo-Optical Instrumentation Engineers (SPIE) Conference Series, Vol. 9907, Optical and Infrared Interferometry and Imaging V, 99070X

Mérand, A., Bordé, P., & Coudé du Foresto, V. 2005, A&A, 433, 1155

Weinberger, A. J., Bryden, G., Kennedy, G. M., et al. 2015, The Astrophysical Journal Supplement Series, 216, 24

Table 1: Basic stellar parameters, null measurements, and zodi levels for the stars observed by the HOSTS survey.

Aperture →										8 pix		13 pix		conservative							
HD number	Name	# SCI	Spectral Type	V (mag)	K (mag)	N' (Jy)	d (pc)	EEID (mas)	fIR/nIR excess	N_{as} (%)	σ_N (%)	N_{as} (%)	σ_N (%)	r_{ap} (pix)	N_{as} (%)	σ_N (%)	aperture for zodi	$N_{as,1}$ (%)	z (zodi)	σ_z (zodi)	z/σ_z
Sensitivity driven sample (Spectral types A to F5):																					
33111	β Eri	2	A3 IV	2.782	2.38	3.7	27.4	248	N/N	-0.004	0.110	0.168	0.119	18	0.372	0.176	13 pix	5.27×10^{-3}	31.9	22.6	1.4
38678	ζ Lep	1/6	A2 IV-V	3.536	3.31	2.1	21.6	176	Y/Y	1.795	0.205	1.609	0.313	25	3.496	0.214	cons.	5.77×10^{-3}	605.8	37.2	16.3
81937	23 UMa	5	F0 IV	3.644	2.73	2.6	23.8	168	N/–	-0.065	0.061	-0.032	0.078	25	-0.135	0.142	13 pix	3.31×10^{-3}	-9.8	23.5	-0.4
95418	β UMa	4	A1 IV	2.341	2.38	4.2	24.5	316	Y/N	0.920	0.055	1.019	0.060	33	1.655	0.102	13 pix	7.45×10^{-3}	136.7	8.0	17.1
97603	δ Leo	4	A5 IV	2.549	2.26	3.9	17.9	278	N/N	0.028	0.051	0.033	0.055	32	-0.013	0.143	13 pix	6.10×10^{-3}	5.5	9.0	0.6
102647	β Leo	2	A3 V	2.121	1.92	6.9	11.0	336	Y/Y	0.470	0.050	0.420	0.054	32	1.160	0.333	8 pix	4.54×10^{-3}	103.5	11.0	9.4
103287	γ UMa	4	A0 IV	2.418	2.43	3.7	25.5	308	N/–	-0.037	0.033	0.003	0.031	34	0.083	0.080	13 pix	8.00×10^{-3}	0.4	3.9	0.1
106591	δ UMa	7	A2 V	3.295	3.10	2.0	24.7	199	N/N	0.453	0.065	0.503	0.082	28	0.924	0.144	8 pix	5.38×10^{-3}	84.2	12.1	7.0
108767	δ Crv	2	A0 IV	2.953	3.05	2.3	26.6	251	N/Y	-0.333	0.131	-0.243	0.199	26	0.933	0.365	13 pix	9.01×10^{-3}	-26.9	22.1	-1.2
109085	η Crv	3	F2 V	4.302	3.54	1.8	18.3	125	Y/N	4.410	0.350	4.580	0.460	24	4.710	0.890	8 pix	2.26×10^{-3}	1952.3	154.9	12.6
128167	σ Boo	3	F4 V	4.467	3.47	1.4	15.8	117	Y/N	-0.019	0.096	-0.006	0.118	22	0.417	0.252	13 pix	2.46×10^{-3}	-2.3	48.0	0.0
129502	μ Vir	3	F2 V	3.865	2.89	2.6	18.3	151	N/N	-0.006	0.092	0.183	0.110	25	0.192	0.198	13 pix	2.64×10^{-3}	69.2	41.8	1.7
172167	α Lyr	4	A0 V	0.074	0.01	38.6	7.68	916	Y/Y	0.055	0.034	0.123	0.038	37	0.392	0.089	cons.	1.18×10^{-2}	33.2	7.5	4.4
187642	α Aql	2	A7 V	0.866	0.22	21.6	5.13	570	N/Y	-0.032	0.166	0.217	0.192	47	-0.995	0.356	13 pix	4.16×10^{-3}	52.1	46.3	1.1
203280	α Cep	1	A8 V	2.456	1.85	7.0	15.0	294	N/Y	-0.301	0.376	-0.233	0.182	18	-0.075	0.266	13 pix	3.91×10^{-3}	-59.6	46.6	-1.3
Sun-like stars sample (Spectral types F6 to K8):																					
9826	υ And	2	F9 V	4.093	2.84	2.4	13.5	136	N/N	-0.245	0.079	-0.287	0.090	24	-0.276	0.169	13 pix	2.20×10^{-3}	-130.3	40.8	-3.2
10476	107 Psc	3	K1 V	5.235	3.29	2.0	7.53	90	N/N	-0.028	0.083	-0.027	0.122	21	0.154	0.181	13 pix	9.45×10^{-4}	-28.3	129.4	-0.2
10700	τ Cet	2	G8 V	3.489	1.68	5.4	3.65	182	Y/Y	0.074	0.079	-0.014	0.084	27	-0.562	0.446	13 pix	1.90×10^{-3}	-7.5	43.8	-0.2
16160	GJ 105 A	1	K3 V	5.815	3.45	1.5	7.18	73	N/–	0.228	0.232	-0.227	0.239	18	0.538	0.363	13 pix	7.12×10^{-4}	-319.2	336.2	-0.9
22049	ϵ Eri	4	K2 V	3.721	1.67	7.4	3.22	172	Y/N	0.144	0.068	0.240	0.066	27	0.463	0.087	cons.	1.56×10^{-3}	296.6	55.6	5.3
30652	1 Ori	4	F6 V	3.183	2.08	4.8	8.07	205	N/N	0.078	0.098	0.107	0.101	28	0.016	0.165	13 pix	2.78×10^{-3}	38.4	36.2	1.1
34411	λ Aur	2	G1 V	4.684	3.27	1.8	12.6	105	N/–	-0.210	0.095	-0.108	0.079	22	0.041	0.136	13 pix	1.57×10^{-3}	-69.1	50.6	-1.4
48737	ξ Gem	3	F5 IV-V	3.336	2.13	4.3	18.0	196	–/N	0.048	0.099	0.124	0.098	27	0.057	0.229	13 pix	2.73×10^{-3}	45.4	35.9	1.3
78154	13 UMa	3	F7 V	4.809	3.53	1.2	20.4	99	N/–	0.369	0.102	0.398	0.144	22	0.028	0.181	13 pix	1.89×10^{-3}	210.1	75.8	2.8
88230	GJ 380	2	K8 V	6.598	3.21	1.9	4.87	65	N/–	-0.111	0.059	-0.077	0.056	20	-0.189	0.087	13 pix	4.19×10^{-4}	-184.7	134.2	-1.4
89449	40 Leo	2	F6 IV-V	4.777	3.65	1.1	21.4	98	N/–	0.238	0.263	-0.018	0.290	21	1.278	0.578	13 pix	2.19×10^{-3}	-8.4	132.5	-0.1
102870	β Vir	4	F9 V	3.589	2.31	4.3	10.9	173	N/N	-0.069	0.039	-0.054	0.049	26	-0.172	0.098	13 pix	2.11×10^{-3}	-25.5	23.0	-1.1
120136	τ Boo	4	F6 IV	4.480	3.36	1.7	15.6	114	N/N	0.111	0.108	-0.112	0.111	22	0.300	0.216	13 pix	2.09×10^{-3}	-53.8	53.0	-1.0
126660	θ Boo	5	F7 V	4.040	2.81	3.1	14.5	147	N/–	0.280	0.052	0.329	0.066	24	0.441	0.083	8 pix	1.89×10^{-3}	148.2	27.7	5.4
141004	λ Ser	2	G0 IV-V	4.413	2.98	2.4	12.1	121	N/N	0.015	0.036	0.025	0.047	23	-0.107	0.117	13 pix	1.68×10^{-3}	15.1	28.1	0.5
142373	χ Her	3	G0 V	4.605	3.12	2.0	15.9	111	N/N	-0.063	0.052	0.112	0.061	22	0.071	0.083	13 pix	1.63×10^{-3}	69.1	37.2	1.9
142860	γ Ser	4	F6 IV	3.828	2.63	2.9	11.3	151	N/N	0.037	0.044	-0.009	0.058	25	0.023	0.079	13 pix	2.35×10^{-3}	-3.7	24.6	-0.2
157214	72 Her	4	G0 V	5.381	3.84	1.0	14.3	79	N/–	0.713	0.146	0.600	0.173	20	0.674	0.193	8 pix	1.21×10^{-3}	587.5	120.5	4.9
173667	110 Her	5	F6 V	4.202	3.03	2.2	19.2	131	N/Y	0.152	0.070	0.194	0.087	24	0.621	0.120	cons.	2.64×10^{-3}	234.9	45.4	5.2
185144	σ Dra	2	G9 V	4.664	2.83	2.7	5.76	113	N/N	0.027	0.052	-0.075	0.071	22	-0.096	0.096	13 pix	1.25×10^{-3}	-60.2	56.9	-1.1
201091	61 Cyg A	4	K5 V	5.195	2.36	4.4	3.49	106	N/N	0.060	0.053	0.047	0.050	22	0.126	0.231	13 pix	7.00×10^{-4}	66.7	71.3	0.9
215648	ξ Peg A	3	F6 V	4.203	2.90	2.2	16.3	132	N/N	0.154	0.121	0.226	0.167	23	0.198	0.214	13 pix	2.22×10^{-3}	101.7	75.0	1.4
222368	ι Psc	2	F7 V	4.126	2.80	2.4	13.7	137	N/–	-0.099	0.127	0.016	0.133	23	-0.062	0.271	13 pix	2.24×10^{-3}	7.2	59.4	0.1